ISSN 1063-7745, Crystallography Reports, 2022, Vol. 67, No. 1, pp. 3–17. © Pleiades Publishing, Inc., 2022.
Russian Text © The Author(s), 2022, published in Kristallografiya, 2022, Vol. 67, No. 1, pp. 5–20.

REVIEWS

Compact Neutron Sources for Condensed-Matter Physics in Russia and Abroad: State of Affairs and Prospects

K. A. Pavlov[a,b,*], P. I. Konik[a], N. A. Kovalenko[a], T. V. Kulevoy[c], D. A. Serebrennikov[d], V. V. Subbotina[a,b], A. E. Pavlova[a,b], and S. V. Grigorev[a,b]

[a] *Petersburg Nuclear Physics Institute named by B.P. Konstantinov, National Research Centre "Kurchatov Institute," Gatchina, Leningradskaya oblast, 188300 Russia*

[b] *St. Petersburg State University, Peterhof, St. Petersburg, 198504 Russia*

[c] *Institute for Theoretical and Experimental Physics named by A.I. Alikhanov, National Research Centre "Kurchatov Institute," Moscow, 117218 Russia*

[d] *Immanuel Kant Baltic Federal University, Kaliningrad, 236041 Russia*

**e-mail: fairy.neutrons@yandex.ru*

Received October 8, 2020; revised November 30, 2020; accepted November 30, 2020

Abstract—A concept of a project of compact neutron source (CNS), dedicated for academical research and industrial application (DARIA), is presented. Several versions of neutron source optimization aimed at increasing the neutron flux and luminosity on a sample are considered. A new approach aimed at designing CNS DARIA is formulated: from a sample to a proton source. Thus, with allowance for the real physical and technical limitations, all CNS elements (proton accelerator, target–moderator–reflector (TMR) assembly, moderators, and neutron stations) are optimized as a whole, and each channel leading to the neutron scattering system is optimized separately as well. The complex of neutron systems includes an inverse-geometry spectrometer, an epithermal diffractometer, a system of small-angle neutron scattering (SANS), and a multispectral diffractometer. The results of calculating the TMR assembly are presented. Starting points for further optimization are established. The advantages and drawbacks of pulsed and cw linear accelerators are described, and the optimal parameters of proton accelerator for CNS DARIA are chosen.

DOI: 10.1134/S1063774522010096

CONTENTS

INTRODUCTION

Traditional particle sources for neutron instruments are either nuclear reactors [1, 2] or proton accelerators equipped with a corresponding target. Neutrons are selected in many various nuclear reactions, but only two of them—fission of heavy nuclei and spallation reactions—possess a favorable combination of a high neutron yield and low energy release per reaction event.

Historically, the technology of creating nuclear reactors was the first to be mastered, and this circumstance determined their active use for studying matter by means of neutron scattering. Characteristic features of these reactors are a compact core, relatively high thermal power, and the presence of special moderator and reflector. In view of the technological limitations on heat removal from the reactor core, the potential of the sources of this type has apparently been exhausted.

Sources based on proton accelerators are more promising. Protons of high energies (on the order of several GeV) bombard a tungsten or mercury target. The number of free neutrons obtained in this process per 1 J heat release is several times higher than in the

fission reaction. In addition, since proton accelerators operate in the pulsed mode, one can naturally apply the time-of-flight technique of neutron measurements, thus using efficiently the generated neutrons. A polychromatic beam is an undoubted advantage of sources of this type for most experiments.

The latest pulsed neutron source—European Spallation Source (ESS) in Sweden [2], whose construction is under way, has reached the limit of spallation technology. The further development of pulsed sources can suggest only a twofold increase in power as compared with ESS. At the same time, the production of free neutrons in spallation reactions remains one of the most efficient known techniques from the point of view of heat release per produced neutron. To ensure further development of neutron sources, one must analyze possible ways to increase the neutron production efficiency.

The ESS, being designed as a long-pulse source, behaves in some respects as a continuous source. It is known that the optimal intermediate pulse duration should correspond to the neutron thermalization time in the moderator. However, the ESS has been designed to operate simultaneously with 24 instruments of different types, which calls for compromises. Throughout optimization of the facility (from source to detector) without any additional constraints would provide an additional gain. The most efficient use of neutrons could be implemented by tuning the source parameters, proceeding from the needs of each specific system or even a separately taken experiment; however, this cannot always be implemented under conditions of a large shared-use center.

Currently, there are two first-class operating neutron sources in Russia: the fast pulsed reactor (IBR-2M) in Dubna [3] and the source on the high-current proton accelerator (IN-06) at the Institute of Nuclear Research of the Russian Academy of Sciences in Troitsk [4]. In 2018 the PIK research reactor (Gatchina) was launched [5]; its characteristics are similar to the reactor of the Institute Laue–Langevin (ILL) [6].

The preparation and performance of neutron scattering experiments on high-flux neutron sources imply the existence of an established community of users. To train them, a network of neutron sources in the immediate vicinity of large scientific centers and Universities must be formed. To answer this challenge, the interest in the so-called compact neutron sources (CNSs) rapidly increases throughout the world [7].

A CNS is considered to be a system aimed at forming and extracting neutron beams, which can accommodate from one to six experimental research stations. In contrast to conventional neutron sources, whose characteristic scale is comparable with that of a scientific institute or a whole collaboration, CNS is positioned on the scale of a university [8] or commercial laboratory. Low-energy nuclear reactions are generally used in compact sources. The most popular version is that where a beryllium target is bombarded by proton beams with energies of about 10 MeV. This solution is a compromise between the increase in neutron fluence and simplification of the technologies in use: among possible candidates, beryllium has the least chemical activity and radioactivity, and the energies are limited by the threshold value for the occurrence of tritium in reaction products (13.3 MeV). Note that, when building the most powerful neutron sources, the direct consumptions on neutron instruments are about 20% of the total cost of building. Hence, the basic way to reduce the neutron source cost is to reduce the cost of the proton accelerator and target assembly.

The existing and projected CNSs can be separated into two classes. The first includes university-type sources [8–11], whose cost is relatively low; they are often based on existing buildings and separate units. These sources make it possible to train students in neutron scattering techniques, perform research that does not call for a high luminosity, and develop new experimental techniques. The second class includes planned intermediate-power sources [12].

It was shown in [12] that, having provided complete joint optimization of all CNS elements (accelerator, target, moderator, neutron instrument), one can obtain a luminosity on a sample that is not inferior to the modern reactors of intermediate and even high power. These sources are proposed to be used as highly efficient centers for collective-use research and training experts.

Thus, the development and creation of a domestic CNS is an important problem both for the formation of an expert community in neutron scattering and for developing neutron techniques. The essential distinctive features of the Russian development of CNS are its integral design and the possibility of complete optimization and adjustment of all systems (including the source elements) for needs of neutron scattering experiments.

1. OPTIMIZATION OF CNS

The efficiency of neutron instruments is determined by the neutron fluence on a sample. Since modern neutron sources have practically reached the upper limit for the existing technologies, one can hardly increase the total neutron flux from a source. For this reason, the development of experimental techniques in the last decade was based on designing and improving the neutron optics and neutron transport systems. Various technical solutions for transporting a neutron flux at distances up to several hundreds of meters with minimal losses have been developed, for example, diverse optical devices based on neutron mirrors and magnetic systems.

The neutron optics used to form a beam sets a phase volume element (wavelength, cross section, divergence, temporal structure) adapted to the experimental scheme implemented in the device. Having optimized the entire optical channel (from radiation capture to the sample), one can reach a gain of 10 to 20 times in the luminosity in comparison with nonoptimal neutron guides of outdated configurations. Such an optimization was performed when reconstructing the neutron-guide systems on the high-flux reactor HFR at the ILL (France) [6] and the neutron source ISIS at the Rutherford–Appleton Laboratory (RAL) (the United Kingdom) [13]. Currently, experts in neutron optics continue their developments aimed at improving classical optical coatings and forming spin-manipulation phase-optical devices; their efforts are promoted by the active development of technologies and materials and wide application of numerical optimization methods.

The first attempt to expand the optimization approach was the design of a neutron source at the ESS. The elaboration of all optical systems was supplemented with some steps to adapt the characteristics of the source and neutron moderator to the needs of the scientific devices located on it. The long pulse duration allows one to extract the so-called stored neutrons, which yields a multiple gain in radiation intensity, but with deterioration in resolution. These solutions lead to a giant increase in luminosity in the experiments calling for a cold-neutron beam with a low spectral resolution. Examples are the techniques implying the scattering from nanostructures, biological objects, and conglomerates, i.e., the techniques that are most urgent in condensed-matter studies. Thus, the ESS implements the concept of increasing the efficiency of scattering methods by designing a source for specific experimental methods—in the form acceptable for a stock of 24 diverse research facilities.

It is necessary to develop (based on the foreign experience) a Russian prototype of CNS that would replace the technologically outdated reactors of intermediate and low power. The novelty of the CNS DARIA project is in application of the concept of integral approach to the entire development cycle. Previously the integral approach was considered as the optimization of the entire neutron optics from source to sample; the application of this approach made it possible to increase multiply the luminosity of systems in many foreign centers. With this approach extended to the logical limit, the accelerator and moderator parameters will be optimized for a specific neutron technique. The entire process of source development is started from the sample towards the neutron source and then to the proton source, in contrast to the previously practised design of systems proceeding from the specific features of neutron source.

2. CNS INSTRUMENTAL STOCK

The complex of neutron scattering facilities satisfies all main needs of neutron community; it includes the following systems: time-of-flight spectrometer INDIrect GeOmetry (INDIGO), operating in inverse geometry and aimed at obtaining data on the structure and dynamics of matter; epithermal diffractometer (ЕПИD) for studying the crystal and magnetic structures of materials; small-angle neutron scattering (SANS) system LArge Scale Structure Observer (LASSO) for studying nanostructures and nanoobjects; and multispectral diffractometer MONOPOLY for investigating mono- and polycrystalline samples using thermal and cold neutrons.

2.1. Spectrometer INDIGO

The main characteristic of the inverse-geometry spectrometer INDIGO is the solid angle within which the scattered radiation is detected. The secondary spectrometer INDIGO is composed of two hemispheres, consisting of many crystal analyzers installed to make the solid angle as large as possible. A cylindrically shaped position-sensitive detector is located under the multianalyzer system (Fig. 1a).

2.1.1. Numerical simulation of spectrometer INDIGO

The block diagram of time-of-flight inverse-geometry spectrometer was modeled in the McStas package. The flight base length from the pulse generator to the sample is 24.2 m; the chopper with a rotation speed of 100 Hz generates 60-μs pulses. The parameters of the secondary spectrometer are as follows: the distances from the sample to the analyzer crystal and from the sample to the detector are 0.4 m. The system consisting of analyzer crystals (PG 002) selects neutrons with a final energy of 3.6 meV, emerging at an angle of 45°.

When simulating the experiment, the final neutron energy was fixed, and the energy transfer was varied in range from 10 to 320 meV. Experimental and analytical dependences of the relative energy resolution on energy transfer were obtained (Fig. 1b). The dependence obtained by numerical Monte Carlo simulation (using the McStas package) coincides well with the curve calculated analytically by the method proposed in [14] at large energy transfers. At small energy transfers the analytical values exceed strongly those obtained numerically, because the experiment was simulated taken into account only the contribution of the pulse duration, with other contributions disregarded. The plot shows also the analytically calculated contributions, which affect the general form of the energy resolution curve. The contribution from L_1 is zero, because the flight base direction makes an angle of 90° with the moderator plane in the CNS DARIA. The uncertainty in pulse duration is the largest term in

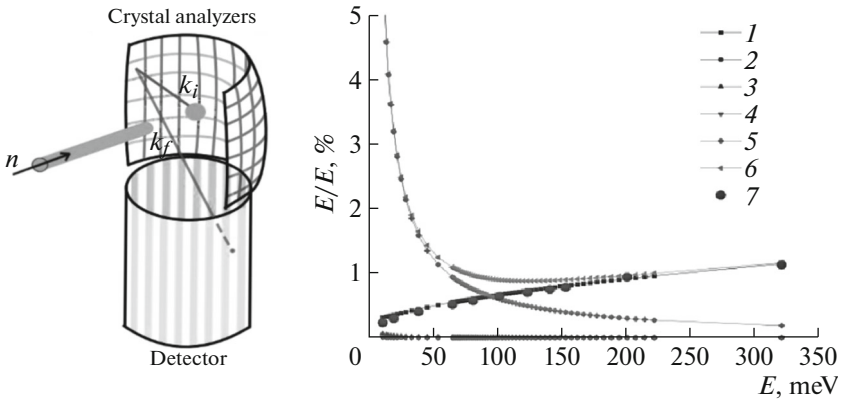

Fig. 1. (a) Configuration of the secondary spectrometer. (b) Dependence of the relative energy resolution on the energy transfer: contributions from the (*1*) time of flight, (*2*) sample thickness, (*3*) analyzer thickness, (*4*) detector thickness, and (*5*) finite transverse dimensions of the detector and sample; (*6*) analytically calculated contribution; and (*7*) contribution simulated by the Monte Carlo method.

the resolution in the larger part of range. This contribution increases with an increase in the neutron energy transfer. At small energy transfers the main contribution is from the uncertainty in R_2, which is determined by the finite sizes of the sample and detector. The smallest contribution is from the uncertainty in the thicknesses of the detector and sample. In this stage the uncertainty in the analyzer thickness does not make any significant contribution; however, when implementing a multianalyzer system composed of many crystals in the McStas program, this contribution will play an important role (with allowance for the increase in the total analyzer area).

Due to the possibility of controlling neutron energy, one can perform an experiment with both cold and thermal neutrons. If cold neutrons are needed, one can use mesitylene with a temperature of 150 K as a moderator. In this case, the source brightness is $B = 6.93 \times 10^{10}$ n/(s cm^2 sr); for a wavelength range of 0.5–4.7 Å and a pulse generation rate of 38 Hz, the fluence is $\Phi = 1.8 \times 10^6$ n/(s cm^2). This value is an order of magnitude smaller than that for the time-of-flight spectrometer TOSCA, ISIS [15]. However, when the wavelength spectrum of the incident beam in such spectrometers must be narrowed, a cascade of choppers is used; in this case the intensity decreases by a factor of 2 due to the cutting off unnecessary wavelengths, and the neutron beam is used inefficiently. The CNS DARIA allows one not only to change the wavelength range to a desired one but also increase the pulse generation frequency. Thus, using the thermal moderator at a temperature of 300 K, a wavelength range from 0.5 to 1 Å, a pulse generation frequency up to 320 Hz, and a source brightness $B = 9.63 \times 10^{10}$ n/(s cm^2 sr), one has the fluence $\Phi = 1.5 \times 10^7$ n/(s cm^2), which corresponds to the fluence on the TOSCA spectrometer. However, the pulse durations for the INDIGO and TOSCA are 60 and 50 μs, respectively; therefore, the energy resolution will be worse than for the ESS spectrometer.

Thus, due to the possibility of controlling the source parameters, the inelastic-scattering spectrometer INDIGO provides higher neutron fluences on the sample.

2.2. Epithermal Diffractometer επιD

The time-of-flight neutron diffractometer επιD is designed for structural studies based on neutron scattering mainly from the epithermal region of source spectrum. At interplanar spacings characteristic of crystalline solids, the epithermal-neutron scattering occurs at small angles in the conventional niche of small-angle scattering systems dealing with thermal and cold neutrons (SANS mode). The difference of the επιD diffractometer from time-of-flight SANS instruments is in very strict requirements imposed on the neutron beam collimation; in the design of the detector, which can detect epithermal neutrons with a high efficiency; and, mainly, in the possibility of detecting the contribution of neutron pulse to the time-of-flight diffraction pattern for several tenths of millisecond.

The conventional time-of-flight instruments for detecting diffracted neutrons require a time window of several milliseconds or several tens of milliseconds after each neutron pulse, which is poorly compatible with structural studies under a pulsed impact on a sample (short-pulsed magnetic and electric fields, light pulses, shock-wave effect, etc.). In particular, the achievement of high magnetic field strengths in the range of 30–100 T using pulsed magnets suggests obviously the duration of magnetic field pulse shorter than a millisecond. The characteristic durations of the relatively flat portion of magnetic field strength for pulsed magnets are generally several tens of microseconds. The detection of time-of-flight diffraction pat-

terns in a specified range of interplanar spacings $d_{min} < d < d_{max}$ at specified time-of-flight bases and upper limit of the time of detecting neutrons from one pulse calls for neutrons with corresponding velocities (i.e., with certain energies). For the d ranges typical of neutron diffraction and at spacings in the experimental zone that are characteristic of CNSs, the detection duration shorter than 1 ms leads inevitably to the use of the epithermal part of neutron spectrum.

The most efficient ranges of application of the επιD diffractometer are the study of the magnetic structures of crystals in strong magnetic fields and the analysis of magnetic phase diagrams. In addition, the diffraction of epithermal neutrons will make it possible to investigate the crystalline and magnetic structures of samples containing elements with a high absorption cross section for thermal and cold neutrons (Gd, Cd, B, Eu, Sm, etc. [16]); in this case, conventional diffractometers can be applied only to samples synthesized with addition of certain isotopes. This approach is very expensive and cannot be always implemented in practice. Many samples inaccessible for classical neutron diffraction and SANS can be considered as quite accessible for the επιD diffractometer.

The operability of the concept of epithermal neutron diffractometer in combination with pulsed magnets was experimentally verified on the time-of-flight EXCED system, which successfully operated in the 2000s, until the KEK source (Japan) was decommissioned [17, 18].

Along with the analysis of epithermal spectral region, the επιD diffractometer will make it possible to carry out structural studies using hot and thermal neutrons. In this case, the small-angle epithermal-neutron detector will be supplemented with a conventional detector operating at the angles typical of classical neutron diffractometers.

The limitations on the resolution in the momentum space, imposed by the beam diffraction at small angles, make impossible design of epithermal diffractometers with a high resolution, even if the angular divergence of the incident and scattered beams and the effective angle of the detector pixel amount to a tenth of degree. For this reason the επιD diffractometer is assigned to diffractometers with a low resolution in momentum transfer and in low relative resolution in the interplanar spacing ($\delta d/d$). This drawback is compensated for by the access to very strong magnetic fields (and other high-amplitude pulsed impacts) and relative transparency of many samples.

The επιD diffractometer calls for a pulsed neutron source with a peculiar spectral energy distribution, the use of a moderator of conventional thickness for it is obviously nonadvantageous. Thus this device is poorly compatible with pulsed sources: shared-use centers with many instruments based on thermal or cold neutron beams. The CNS is excellently suitable for optimizing the target block and moderator in order to generate a high fluence of neutrons with energies of several electronvolts or several tens of electronvolts without providing a high fluence of lower energy neutrons. Along with the επιD, epithermal beams can be used in neutron radiography (tomography) and medical applications (for example, neutron-capture therapy, for which epithermal neutrons possess an optimal combination of penetrating ability and degree of biological impact). The επιD diffractometer can be installed on a specialized compact source of epithermal neutrons or on the DARIA source, with the epithermal option provided (presence of a specialized removable moderator or specialized segment of moderator unit).

An advantage of a time-of-flight pulsed neutron diffractometer is the relative simplicity of its basic design (Fig. 2a). Specifically, in the simplest case a diffractometer of this type consists of only three structural elements: collimator, sample unit, and detector; it does not contain a monochromator, which is an integral part for a majority of classical diffractometers.

The registration of a neutron by a specific detector pixel sets the scattering angle (2θ), and the energy of elastically scattered neutrons arriving at the detector is determined by the time of their flight. Undoubtedly, this realization is possible on only a pulsed neutron source, in which the pulse onset time is clearly specified. In the case of a stationary source, the basic design of diffractometer is complicated due to the addition of a chopper cascade.

A specific feature of application of epithermal neutrons is that one must use small scattering angles 2θ to measure magnetic Bragg reflections at a scattering vector on the scale $Q = 1$ Å^{-1} ($d \approx 6.283$ Å), which is typical of most of antiferromagnetic structures. For example, as was shown in [17, 18], where the world's only specialized epithermal neutron diffractometer EXCED was described, at $Q = 1$ Å^{-1}, resolution $(\Delta Q/Q) = 10\%$, and neutrons with energy $E = 1$ eV, the scattering angle 2θ is only 2.6°. In this case, it is of great importance to provide a relatively extended time-of-flight base and a high degree of neutron beam collimation. The path length is primarily determined proceeding from the desired resolution in the Q space:

$$\frac{\Delta Q}{Q} = \sqrt{\left(\frac{\Delta t}{t}\right)^2 + \left(\frac{\Delta L}{L}\right)^2 + (\Delta\theta\cot(\theta)^2}. \qquad (1)$$

It is also obvious that the neutron path length is significantly limited by the spatial dimensions of the room in which the installation is placed. At a long first path length L_1 (for example, L_1 is 6.4 m in the EXCED diffractometer) and small angles θ, the first and second terms in Eq. (1) can be neglected, whereas the third term is dominant. In this case, the desired resolution in the Q space can be estimated as $\Delta\theta\cot\theta$. In particular, for the angles $\theta = 1°$, 2°, and 5° the resolution is $57.3\Delta\theta$, $28.6\Delta\theta$, and $11.4\Delta\theta$, respectively.

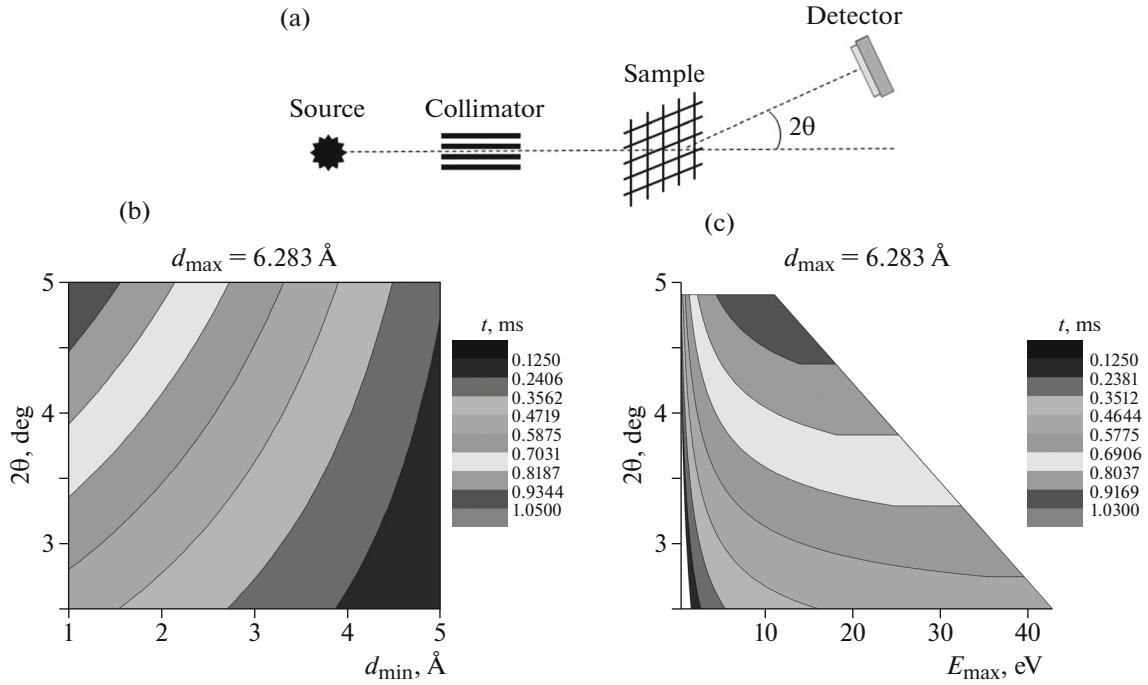

Fig. 2. (a) Schematic of the simplest time-of-flight diffractometer επιD. (b) Calculation of the pulse duration in dependence of the scattering angle 2θ and range of measured interplanar spacings *d*. (c) Calculation of the pulse duration as a function of the scattering angle 2θ and neutron energy *E*.

Thus, the arm length L_2 is determined proceeding directly from the desired resolution, range of covered angles, and detector angular size.

As was indicated above, for a sample subjected to a pulsed physical effect, the pulse duration on the sample is a priori assumed to be shorter than 1 ms. The pulse duration on the sample is considered to be the total time of flight through the sample for all neutrons with different energies in the same source. These neutrons are directly detected when measuring a time-of-flight diffraction pattern. In view of this, particular attention must be paid to the estimation of the pulse duration on the sample in dependence of the geometry of the system, range of measured interplanar spacings, and the source spectrum. The plots reported below show the results of calculating the pulse duration on the sample both in the scan over the range of measured interplanar spacings *d* and in the scan over neutron energies *E*. In both cases the maximum interplanar spacing was measured to be $d_{max} = 6.283$ Å, the angular range was taken to be $2.5° < 2\theta < 5°$, and $L_1 = 6.4$ m (in analogy with the EXCED diffractometer).

The data in Figs. 2b and 2c suggest the following: a short pulse duration (less than 1 ms) on the sample can be obtained by only limiting the range of measured interplanar spacings *d*, which, in turn, is equivalent to the use of a fairly narrow energy range for epithermal neutrons.

An alternative solution is the possibility of applying a two-dimensional positional-sensitive detector. In this case, the time-of-flight technique also makes it possible to measure diffraction patterns in the scan in momentum transfer using a nonmonochromatic beam. In particular, at scattering angles $2° \le 2\theta \le 10°$ and neutron energies in the range of 1.7–2.7 eV, the pulse duration on the sample is only several tens of microseconds. The next stage of calculations of device parameters implies the existence of detailed information about the neutron source spectrum, fluence, and limitations imposed on the spatial dimensions of the entire system.

2.3. Small-Angle Instrument LASSO

Currently, SANS is one of the most popular research techniques used in condensed matter physics [19].

The essence of this method is the detection of neutrons scattered at small angles (on the order of few degrees). To implement it, one needs a spacing of several tens of meters between the sample and detector in order to distinguish between the beam fraction scattered from the sample and the direct beam passed through the sample without interaction. The instrumental accuracy of angular measurements is generally provided by the high degree of collimation of the beam incident on the sample. The only way to collimate neutron beams is to absorb neutrons whose divergence exceeds the desired level; therefore, the experiment is

characterized by a low luminosity and, as a consequence, low measurement statistics for weakly scattering samples. Focusing a neutron beam in order to increase the device sensitivity is hindered in the general form, because it deteriorates the resolution of measurements, with an insufficient gain in luminosity. However, focusing is used in some cases. The basic principles of constructing small-angle systems and calculating their instrumental resolution are known well; they have been described in several fundamental works [19–21].

One can use the time-of-flight measurement technique to expand the measurement range in the momentum transfer. In this case, time-resolved detection of polychromatic beam scattering is performed; the detection results are used to find directly the wavelengths of the neutrons arriving at the detector at each instant. This technique, being also used to solve a number of problems on stationary sources, is natural for pulsed sources, because the beam has initially a pulsed temporal structure, and one has only to decipher it to gain additional information. Here, a well-known problem is the dependence of the scattering cross section of neutrons on their wavelength; nevertheless, it can be solved at the software level when processing primary data. Note that the beam polychromatism and temporal structure can be used not only to increase the measurement range but also as an instrument for expanding significantly the potential of the SANS method (from the structural to the dynamic version) [22].

Since the design of CNS suggests its low power, the implementation of SANS method with a monochromatic beam on it appears to have no sense, because the luminosity of the experiment will be insufficient to solve most of modern problems. The focusing geometry is most efficient for a neutron beam; however, it calls for a highly advanced optics. It was decided to implement this measurement scheme in the LASSO system along with the main (reflectometric) operation mode, which requires similar manipulations with the beam.

The composition of the installation is as follows.

1. Cold moderator. It provides primary formation of a neutron beam, having maximum energy in the cold spectral region and a high brightness in a specified direction.

2. Chopper cascade. It consists of at least three choppers: generator, long-wavelength limiter, and overlap filter. It forms a clearer pulsed beam structure (initially roughly specified by the source and filters the spectrum to the specified wavelength range.

3. Collimation system. It consists of several pairs of controlled diaphragms of variable size and a set of removable collimator/neutron guide sections, placed in an evacuated chamber. This system allows one to choose a desired neutron beam divergence on a sample from a set of several available values.

4. Sample unit. It contains a holder of several samples with their automatic feeding into the beam and a set of systems for specifying experimental conditions (furnace, cryostat, magnet, high-pressure cell).

5. Wide-aperture position-sensitive detector (PSD). It is placed in an evacuated chamber, where it is automatically fixed in one of several positions, providing measurements in matched momentum transfer ranges.

6. Optional elements of the system:

(i) removable bender for line-of-site departure and beam polarization;

(ii) polarization equipment, including two flippers and polarizing analyzer based on a magnetic lens.

2.3.1. Calculation of pulsed beam structure for classical geometry

The dimensions of the system and operating wavelength range were chosen semiempirically as most demanded in modern SANS studies and, at the same time, available for application on the CNS. Neutrons with wavelengths on the order of 20 Å and collimation bases of 20 m are considered as inappropriate due to the expected low luminosity. Therefore, the system has dimensions of 10 + 10 m and an operating wavelength range from 5 to 15 Å, from which a band of desired width is chosen, for example 5–10 or 8–12 Å. The total path length from the first chopper to the detector in the calculations was taken to be 25 m, with a margin for the sample environment system, near-target communications, and polarization technique. The desired pulse frequency is the inverse time of flight for the slowest neutrons. The linear neutron velocity, calculated as for the wavelength of 15 Å, amounts to 263 m/s. The time of flight for a distance of 25 m at this velocity is 95.1 ms; i.e., the pulse frequency of 10 Hz with a small margin provides non-overlapping pulses.

The desired pulse duration is determined by the specified instrumental resolution. The resolution in the momentum transfer, typical of SANS, is $q \sim 10\%$. The angular and spectral contributions to the resolution are of equal weight:

$$\left(\frac{\Delta q}{q}\right)^2 = \left(\frac{\Delta\theta}{\theta}\right)^2 + \left(\frac{\Delta\lambda}{\lambda}\right)^2. \quad (2)$$

To obtain a q resolution of 10%, each of these contributions should be 7%. The worst wavelength resolution is determined by the shortest wavelength on the shortest path length. The minimum wavelength is 5 Å, and the minimum flight path length is implemented at the detector position closest to the sample, i.e., at a distance of 15 m from the first chopper. Thus, the pulse duration is equal to the difference in the times of flight on a distance of 15 m for the neutrons with wavelengths of 5 and 5.35 Å (107% of 5 Å). For a wavelength of 5 Å, the velocity is 789 m/s, and the time of

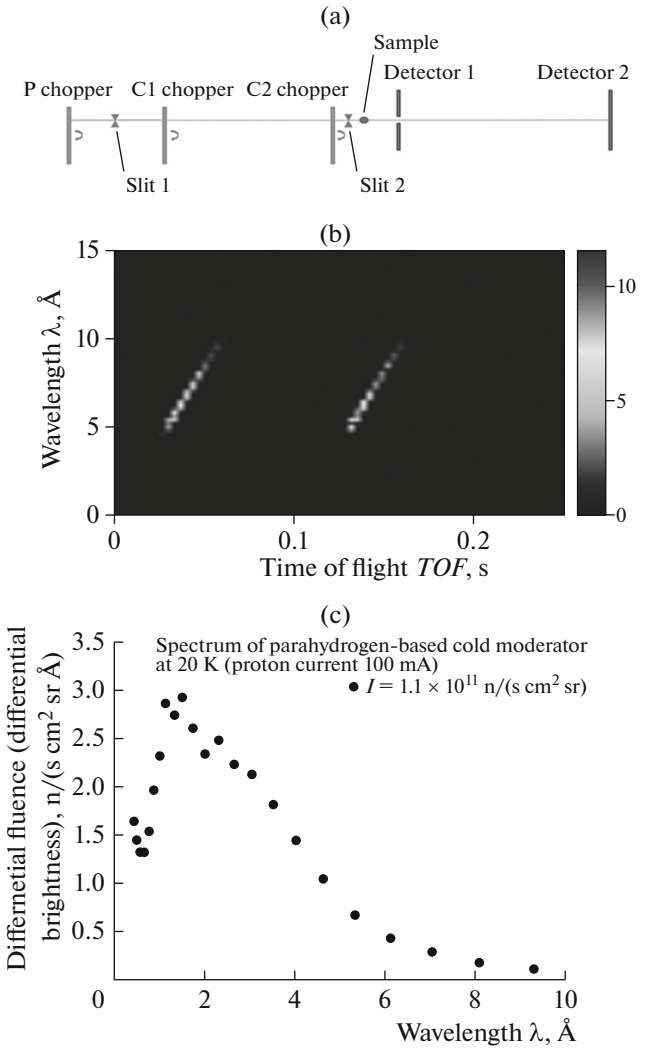

Fig. 3. (a) Schematic of the small-angle system LASSO in the point geometry, (b) example of λ–*t* diagram, and (c) calculation of the cold-moderator spectrum.

flight on 15 m is 19.01 ms. For a wavelength of 5.35 Å, the velocity is 737.4 m/s, and the time of flight on 15 m is 20.34 ms. Thus, the pulse duration optimal for the experiment is 1.33 ms.

To obtain maximum luminosity, the optimal pulse duration should coincide with the moderation time for neutrons with a specified wavelength. For the middle of the wavelength range we chose (5–10 Å), this value is about 150 μs, which is an order of magnitude smaller than the calculated one. The summary pulse duration should to be a compromise between these two values.

A schematic diagram of a small-angle system is shown in Fig. 3. It consists of a P chopper, which forms a pulsed beam structure, two collimating slits, and choppers C1 and C2 for filtering recycled neutrons. There are also two detectors (for large and small momentum transfers) in the system. The width of the P-chopper slit is determined by only the specified resolution and does not affect any other parameters. The angular slit width necessary for obtaining a pulse width of 1.33 ms is 4.8°. Strictly speaking, the main function of the P chopper is already performed by the source due to its initial pulsed structure; however, since the natural pulse shape is unlikely to be convenient for use, one must apply a chopper to correct it.

The slit width and phase of C2 chopper allow one to choose a desired operating wavelength band. The time delay for opening with respect to the P chopper should to be equal to the time of flight of the shortest wavelength neutrons in the band; the closing time should correspond to the time of flight of the slowest neutrons. For example, for a band of 5–10 Å C2 should have a slit with angular width of 63.7° and shifted in phase relative to the P opening by 95.6°. Figure 3b shows a model wavelength–distance diagram at the detector position, calculated for the band of 5–10 Å in the McStas package. One can see that the calculated frequency–phase parameters provide the desired time resolution with a good margin.

The operating wavelength band is a dynamically varied parameter, which should be controlled from experiment to experiment by changing the angular width and phase of C2 chopper. Technically, the simplest way to do it is to use not one disk for C2 but a pair of closely spaced disks, which rotate synchronously, but provide a possibility of changing the phase shift. The specified shift will make it possible to change efficiently the slit width.

The C1 chopper is designed for filtering recycled neutrons with wavelengths multiply exceeding the operating wavelength. A neutron having a twice smaller velocity arrives at the detector not with its "own" pulse but with the next one, which gives rise to a systematic measurement error. In the above-reported example these neutrons have wavelengths not less than 15 Å; thus, taking into account the characteristic shape of the spectrum, their contribution to the recorded intensity is negligible. However, in some cases this contribution may affect the measurement results; therefore, the question about the necessity of using a C1 chopper can be solved finally only after refining the scheme of the experiment and estimating the fluence on the sample.

2.3.2. Monte Carlo simulation

The compiled model (Fig. 3a) includes a source; the above-described set of choppers; a damper neutron guide 4 m long; a collimation system 10 m long, composed of four diaphragms, providing different collimation lengths, and optionally inserted neutron-guide sections; a set of technological gaps (1 m long in total); and 10-m sample–detector flight path. The total source–detector flight path length is 25 m, the sample size (with a slit installed before) is 1.5 × 1.5 cm^2,

and the cross section of the first collimation slit is 3 × 3 cm^2.

The neutron fluence from the source was found by estimating the operation of a cold moderator at a pulsed proton current of 100 mA in the accelerator. A cold moderator based on parahydrogen, placed in a thermal moderator (water surrounded by a beryllium reflector), was used as a source. The source brightness was found to be 1.1 n/(s cm^2 sr) (integral over wavelengths in the range from 0.5 to 15 Å, on the assumption that the source emits isotropically into an angle of 2π). The source area (luminous moderator surface) was assumed to be 55 cm^2 in the estimation; this assumption makes it possible to fill uniformly and with a margin the phase volume necessary for the small-angle experiment. Figure 3c shows the spectrum calculated for the proposed moderator. The wavelength distribution is far from ideal, because the spectrum has a pronounced maximum in the thermal region. However, in the range of interest—from 5 Å and higher—all potentially appropriate moderators (parahydrogen, methane, mesitylene) behave identically in the first approximation; therefore, to make a rough estimation, one can use this spectrum as the simplest for approximation.

Within the developed model we calculated the fluence on the sample in three measurement modes: for collimation bases of 1, 5, and 10 m. The calculated fluences were, respectively, 2.9×10^4, 2500, and 630 n/(s cm^2). Figure 4 presents the results of simulating the beam parameters at the sample point. One can see that the spectrum corresponds to the specified one, which confirms the analytical calculations presented in the previous section. The divergence distribution has a correct shape, which can be easily approximated and allows one to take into account the spectral contribution to the resolution.

The obtained fluences are low to compete with modern sources; however, they provide the minimum luminosity necessary for implementing most of the currently demanded small-angle experiments. This fact proves the fundamental possibility of existence of such a system. In reality, the luminosity can be increased by optimizing the moderator with respect to the spectrum and directional radiation pattern.

Due to the constant rotation speed of the P chopper, the above-described scheme provides detection in the range from 0 to 15 Å, independent of the band chosen. It turns out that, when using a narrow bandwidth, the detector is idle for a significant part of time. On the one hand, this solution simplifies significantly the scheme in the technical aspect and allows one to exclude completely the recycled contribution from consideration. At the same time, this inefficient use of neutrons may be critical under conditions of a compact source with a relatively low luminosity. Tuning of the disk rotation speed (proceeding from the bandwidth in use) would make it possible to use more efficiently the beam and load uniformly the detector. In particular, the time necessary for the scan reported in the example with a band of 5–10 Å is in fact shorter by a factor of 3; i.e., the pulse generation frequency can be increased from 10 to 30 Hz without any loss in the range and resolution and thus reduce thrice the statistics collection time. Technically, this also means that the angular width of the P chopper must be changed;

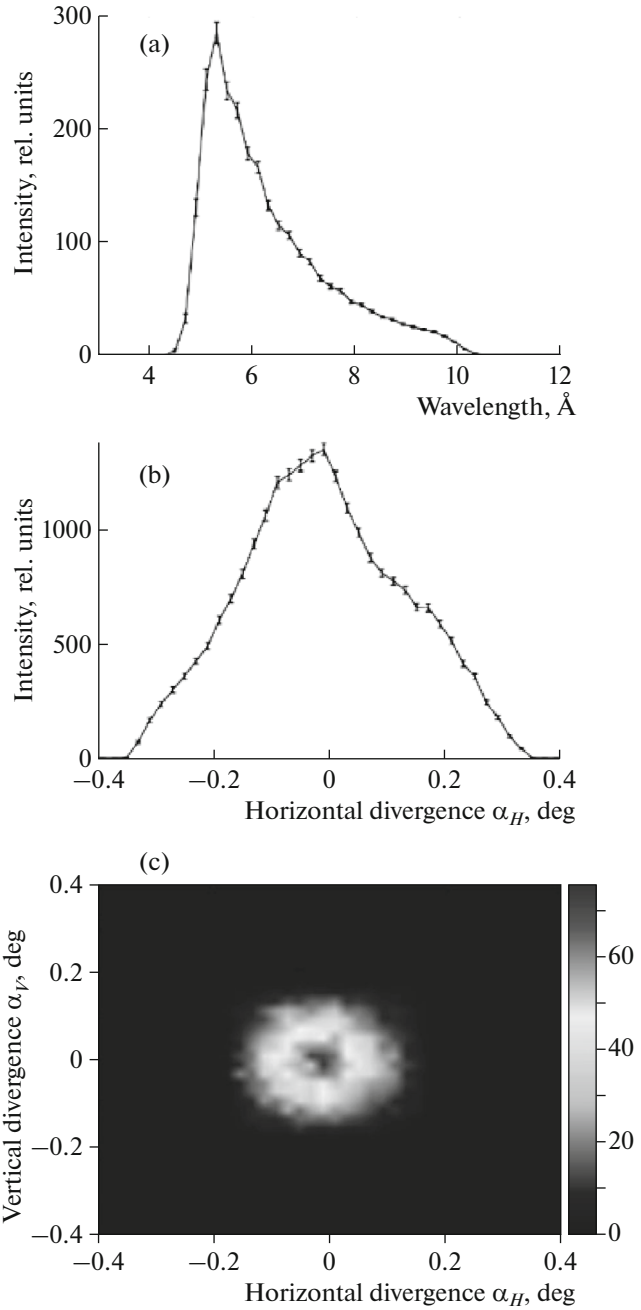

Fig. 4. (a) Time-averaged spectral distribution of neutrons at the sample point for the LASSO system, (b) distribution over horizontal divergence for 5-m collimation, and (c) divergence map for 10-m collimation.

i.e., as well as the C2 chopper, P must be implemented using a pair of disks instead of one.

2.4. Multispectral Diffractometer MONOPOLY

The multipurpose time-of-flight diffractometer MONOPOLY is aimed at studying both single-crystal and powder samples in a wide range of interplanar spacings. Its main components are as follows: mesitylene moderator; cascade of choppers, which serves as a filter of higher order wavelengths and makes the pulse more rectangular; a neutron-guide system, consisting of two (bent and elliptical) optical elements; sample unit; and wide-aperture PSD, which covers a large solid angle.

The concept of this diffractometer has a number of unique features.

First, it is proposed to adapt the proton burst duration to the spectrum in use. Wavelengths of about 1–2 Å and burst durations of about 31–62 μs will be used to study the nuclear structure, and wavelengths of about 5 Å and burst durations of about 155 μs will be applied to analyze the magnetic structure. The burst durations are chosen so as to correspond the retardation time in the moderator. A specific feature of this diffractometer configuration is the constant relative resolution in any operation mode.

Second, a mesitylene moderator, similar to that installed on the IBR-2M reactor, will be used. This moderator can operate in a wide temperature range, due to which a Maxwell spectrum can be adapted to a specific study.

3. TARGET–MODERATOR–REFLECTOR ASSEMBLY

The components of the target–moderator–reflector (TMR) assembly are target, moderator, reflector, and cold moderator. To analyze its geometric parameters, affecting directly the neutron fluence, we performed numerical simulation within the PHITS software using the JENDL-4.0 library. The heat release was calculated using the similarity equations, applicable to the specified cooling conditions.

With conditional parameters of a 13-MeV proton accelerator, maximum current in pulse of 100 mA, and coefficient filling of 5% for a beryllium target (shaped as a cylinder 0.5 cm in radius and 0.2 cm thick and placed in vacuum), we performed a simulation in order to determine the Bragg peak position and the neutron yield. The neutron yield was determined at different target thicknesses. The optimal thickness turned out to be 1 mm. At this value the blistering effect (accumulation of hydrogen in a target exposed to a proton beam) is excluded [23], and the heat release of the target is reduced to 10%; at the same time, the number of neutrons remains practically at the maximum level (Fig. 5a).

The fast-neutron spectrum (Fig. 5b) has an average energy of 3.3 MeV, which is in agreement with the data in the literature on CNSs [24, 25]. The simulation revealed that an increase in the target diameter reduces strongly the neutron fluence from the target in the direction perpendicular to the proton beam direction (Fig. 5e). A possible reason is that, at a larger target diameter, the probability for a neutron generated at the center of the target to leave it in the aforementioned direction without collisions decreases.

The spherical reflector was calculated. It was shown (Fig. 5d) that a beryllium reflector operates more efficiently than a graphite one. At the same time, the beryllium reflector will be smaller in size for the following reason: the operation of a reflector is efficient if its dimensions fit into two or three diffusion lengths; the latter is 22 cm for beryllium and 54 cm for graphite. The presence of a reflector itself increases several times the thermal neutron fluence. The calculation of the reflector implied the presence of a sphere with a water moderator 4 cm in radius.

To date, only parahydrogen and solid methane have been considered as cold moderators; it is planned to compare them with mesitylene. The distribution of cold neutrons is presented in Fig. 5e. Channels with cold moderators were incorporated into the water moderator. Thus, an acceptable density of cold neutrons can be reached at the following moderator sizes: length of 11 cm and radius of 4 cm for parahydrogen and length of 2.5 cm and radius of 4 cm for solid methane. The uncertainty of each simulation in the PHITS program was 2%.

A thermal calculation of the TMR assembly showed that all heat generated in it (6.5 kW) can be removed either using a rotating design or a water flow with a sufficiently high velocity; however, in any case the heat-exchange surface area should exceed the target area irradiated by the proton beam.

To conclude, we should note that the performed calculation of the TMR assembly yielded several reference points for further optimization. Further steps in this direction will be the choice of target diameter, optimization of thermal moderator, and consideration of the mutual influence of channels with cold moderators; the biological shielding of the target will be calculated as well.

4. PROTON SOURCE AND ACCELERATOR

To provide the current scientific and applied research with desired neutron beams, large-scale neutron sources based on high-intensity proton accelerators operate (e.g., IPNS [26], Los Alamos Neutron Science Center [27], ISIS [28], SNS [29], and JPARC [30]) or are being built (ESS [2]). In Russia, the accelerator source IN-06 is successfully operating at the INR RAS [4], and the NEPTUN project is being considered as a neutron-pulse generator [32]. Currently,

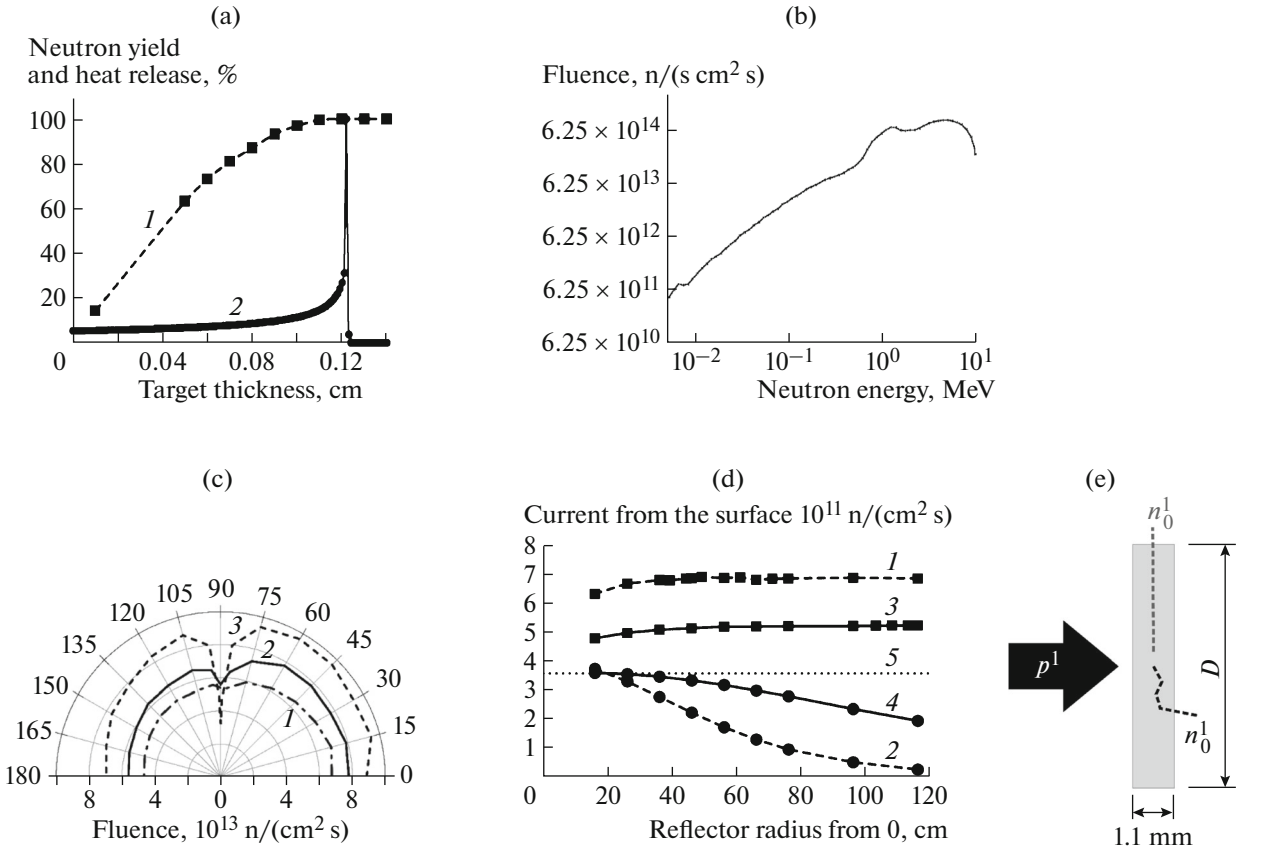

Fig. 5. (a) Dependences of the neutron yield and heat release on the target thickness: (*1*) neutron yield and (*2*) Bragg peak for protons. (b) Distribution of fast neutrons. (c) Angular distributions of fast neutrons for target radii of (*1*) 0.5, (*2*) 5, and (*3*) 1 cm. (d) Comparison of the efficiency of beryllium and graphite reflectors: (*1*) current from the moderator surface to the beryllium reflector, (*2*) neutron leakage from the beryllium reflector surface, (*3*) current from the moderator surface to the graphite reflector, (*4*) neutron leakage from the graphite reflector surface, and (*5*) current from the moderator surface to vacuum (without reflector). (e) Clarification of the probability of neutron escape with an increase in diameter. (f) Model of TMR assembly with a cold-neutron distribution.

along with the large-scale objects, some other projects based on linear accelerators are also being developed: SARAF in Israel [32], FRANZ in Germany [33], MUNES in Italy [34], and BELA in Russia [35].

The project BELA of an interdisciplinary system based on the ECR ion source and a linear accelerator is under development at the Institute of Theoretical and Experimental Physics of the National Research Centre "Kurchatov Institute" (ITEP NRC KI). The technologies developed within this project will be used for commercial production of compact systems based on cw linear accelerators and CNSs for neutron-capture therapy and activation analysis.

The prototype of CNS DARIA was the research reactor BER-II at the Helmholtz-Zentrum Berlin für Materialien und Energie (HZB) (Germany), which provides a neutron beam fluence of 2×10^{14} n/(s cm^2). At proton beam energy of 13 MeV and beryllium target, the necessary ion beam intensity was estimated for three different modes: thermal (pulse duration τ = 44 ms and pulse repetition frequency T = 120 Hz), bispectral (τ = 66 ms, T = 120 Hz), and cold (τ = 110 ms, T = 20 Hz). It was shown that a proton beam with a current of 80–85 mA on the target must be provided. To obtain such a beam current, a high-intensity pulsed linear accelerator must be developed. As an alternative, a linear cw accelerator with a low current, followed by a beam compressor, can be used. This concept is implemented in the Frankfurt Neutron Source at the Stern–Gerlach Zentrum (FRANZ) [33].

4.1. Pulsed Linear Accelerator

A pulsed linear accelerator (Fig. 6a) should have the following components: pulsed high-current ion source; low-energy beam transport (LEBT) system for matching the beam from the ion source before entering the linear accelerator; pulsed high-intensity linear accelerator (both radio-frequency quadrupole (RFQ) focusing and drift tube linear (DTL) accelerator); and high-energy beam transport (HEBT) channel to the target.

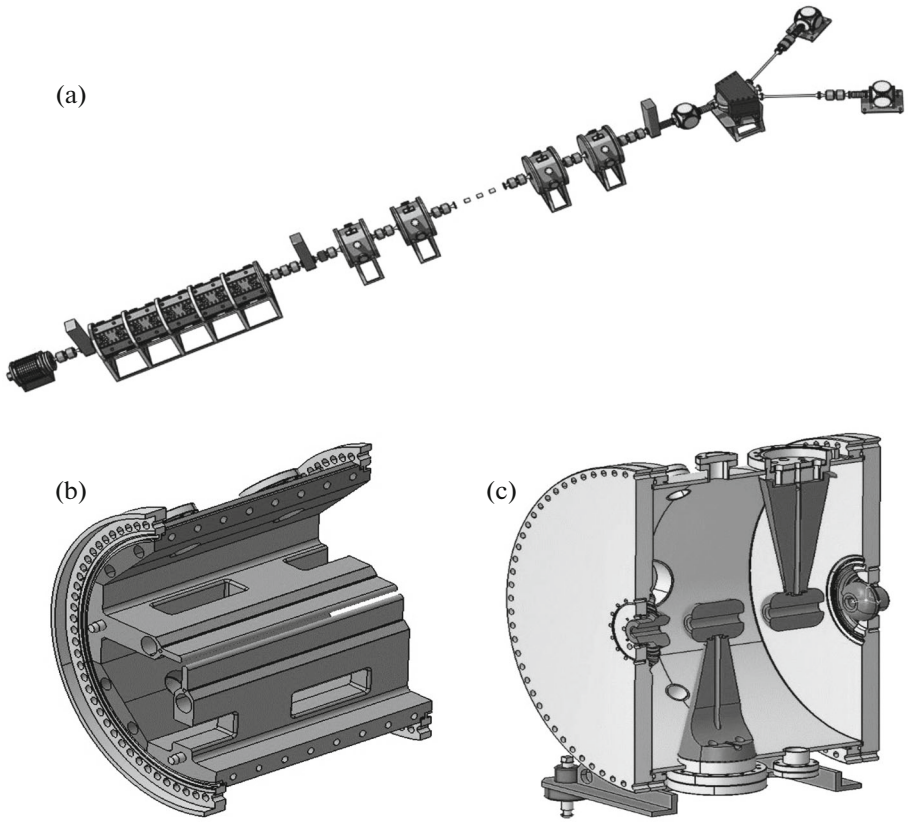

Fig. 6. (a) General view of the linear accelerator for CNS DARIA, (b) schematic of RFQ with shifted windows, and (c) schematic of 3-gap DTL accelerator.

Currently, the ECR ion source provides a dc proton current up to 140 mA [37, 38]; however, sources of this type are very expensive. Pulsed ion sources of different types, such as duoplasmatron or multicusp ion source, can provide the desired ion beam intensity, but they all have a limited lifetime. Moreover, the design of the shaping system and LEBT for such a high-intensity beam is challenging because of the presence of a high space charge.

In addition, the emittance is not a linear function of the beam current; therefore, an increase in the beam intensity leads to a significant increase in the emittance. Since RFQ and DTL operate in the pulsed mode, the maximum electric field on the electrode surface may be ≥1.8 Kp (Kp is the Kilpatrick electric field for a specified frequency in the cavity [39]). This provides a higher acceleration coefficient and a smaller linear accelerator length for a beam with the same emittance. One can also use the relatively low acceptance-to-emittance ratio, which remains equal to three in any case because of the high current force. This circumstance makes it possible to preserve the transverse beam size in the range of linear power of the accelerating channel. Nevertheless, the beam emittance is a function of current; hence, the higher the current, the higher the emittance is. Therefore, the pulsed linear accelerator can be compared with a cw linear accelerator.

4.2. cw Linear Accelerator

cw linear accelerator, along with the equal pulse duration, should have beam compression system on the output channel. A harmonic buncher cannot be used to this end, because its presence attenuates the beam more than twice. In addition, 13-MeV protons should lead to activation of HEBT materials. Therefore, it is necessary to develop a system similar to that applied in the FRANZ.

Concerning the ion source, one can use ECR (current up to 5 mA and frequency of 2.45 GHz) with a system of permanent magnets. This approach significantly simplifies the operation mode and reduces operating costs. The smallness of the beam space charge simplifies the development of both the extraction system and the LEBT. However, to implement the cw operation mode, the RFQ and DTL should be characterized by a lower maximum electric field on the electrode surface (≤1.4 Kp) and a higher acceptance-to-emittance ratio (≥6). Moreover, 100% beam transport through the RFQ and DTL channels is recommended. Any loss in the RF channel of the lin-

Table 1. Advantages and drawbacks of pulsed and cw linear accelerators (neutron sources)

		cw linear accelerator	Pulsed linear accelerator
Ion source	Advantages	Simplicity in operation, reliability, long lifetime	Low cost
	Drawbacks	Relatively expensive in production	Short lifetime, complicated extraction system
LEBT	Advantages	Easily accessible transverse matching	Loss allowable
	Drawbacks	Buncher is necessary for longitudinal matching	Large beam space charge
RFQ (DTL)	Advantages	Low current	$E_{max} \geq 1.8$Kp $a/\varepsilon \leq 3$
	Drawbacks	$E_{max} \leq 1.4$ Kp 100% beam transport $a/\varepsilon^* \geq 6$	High emittance (ε)
HEBT	Advantages		Standard HEBT
	Drawbacks	High-energy beam must be compressed	

* ε is emittance.

ear accelerator may initiate a breakdown, as a result of which electrodes can be destroyed. One can reach 100% transport efficiency and even 100% acceleration only by applying 6D matching of the beam at the input of the linear accelerator. 6D matching can be provided using a harmonic buncher at the RFQ input [39]. It should be noted that, despite the stability to breakdown, it is also desirable to install a harmonic buncher at the input of pulsed linear accelerator.

The advantages and drawbacks of the accelerators of two types are listed in Table 1. It is necessary to perform a detailed study of each linear accelerator to choose the most appropriate one for a neutron source. A detailed study of different accelerators for CNS was started within the DARIA project [41]. The starting point was the development of the first version of cw linear accelerator in the framework of the BELA project.

A detailed description of the first results of simulation of the beam dynamics and electrodynamic characteristics can be found in [41]. A 100% acceleration efficiency was obtained in a linear accelerator. The total length of the linear accelerator is 10.4 m; its operation requires about 1 MW RF power (0.4 MW for RFQ and 0.6 MW for DTL). The RF power was estimated using the RFQ structure with shifted coupling windows and 3-gap DTL [42] (Figs. 6b, 6c). This RFQ structure provides high field stability, which is very important for both a linear accelerator with high intensity pulses and a cw linear accelerator. This structure was successfully used for the cw linear accelerator at the Argonne National Laboratory (USA) [43, 44] and for the world's only superconducting cw linear accelerator at the LNL-INFN (Italy) [45]. It was also used for the high-intensity RFQ at the ITEP [46] and JINR [47]. The 3-gap DTL is a compromise between the necessity of having a short focusing period (therefore, the number of gaps must be as small as possible) and a high figure of merit.

A compact ECR ion source 2.45 is under development at the ITEP for the BELA and DARIA projects. The first experimental results obtained on this source were reported at the conference ICIS-2019 [48].

CONCLUSIONS

Summing up, we should note the constantly increasing interest in neutron techniques and their poor accessibility. Therefore, compact neutron sources are needed to develop neutron scattering methods, train experts, and carry out corresponding experiments in Russia; these sources are expected to provide the neutron community of Russia with neutron beams of desired luminosity and necessary neutron installations.

The Russian CNS DARIA is developed taken into account the experience of foreign colleagues in the creation of pulsed sources. Different versions of optimizing neutron sources in order to increase the neutron fluence and luminosity on a sample were considered, due to which the approach to optimization was expanded to logical limit. Since there is no need to search a compromise for several systems, each channel with a moderator can be optimized for a specific neutron installation. In addition, both the proton accelerator and TMR assembly will be optimized. The complex of neutron installations includes an inverse-geometry spectrometer, an epithermal diffractometer, a SANS system, and a multispectral diffractometer. The results of preliminary calculations for the TNR assembly were demonstrated. Reference points for subsequent optimization were established. The advantages and drawbacks of pulsed and cw linear accelerators were described, and the parameters of proton accelerator for CNS DARIA (proton beam energy and proton current) were chosen to be 13 MeV and 100 mA, respectively.

ACKNOWLEDGMENTS

We are grateful to E.S. Klement'ev, M.V. Bulavin, K.A. Mukhin, and many other researchers from the Immanuel Kant Baltic Federal University, JINR, ITEP NRC KI, and IPF RAS for the help in work and for supplying necessary materials.

FUNDING

This study was supported by the Russian Science Foundation (grant no. 19-12-00363).

CONFLICT OF INTEREST

The authors declare that they have no conflicts of interest.

REFERENCES

1. Reactor Institute TU Delft Website. http://www.tnw.tudelft.nl/en/cooperation/facilities/reactor-instituut-delft/.
2. ESS website: http://europeanspallationsource.se/.
3. JINR Laboratory of Neutron Physics (Dubna) Website. http://flnph.jinr.ru/ru/.
4. S. F. Sidorkin and E. A. Koptelov, Poverkhn.: Rentgenovskie, Sinkhrotronnnye Neitr. Issled., No. 6, 97 (2013).
5. Reactor PIK (PNPI NRC KI, Gatchina) Website. http://www.pnpi.spb.ru/win/facil/pik.htm.
6. Institute Laue–Langevin Website. https://www.ill.eu/.
7. C. Andreani, C. K. Loong, and G. Prete, Eur. Phys. J. Plus. **131**, 217 (2016). https://doi.org/10.1140/epjp/i2016-16217-1
8. C. M. Lavelle, D. V. Baxter, A. Bogdanov, et al., Nucl. Instrum. Methods Phys. Res. A **587**, 324 (2008). https://doi.org/10.1016/j.nima.2007.12.044
9. J. Wei, H. B. Chen, W. H. Huang, et al., *Particle Accelerator Conference TU6PFP035, 2009*. https://accelconf.web.cern.ch/PAC2009/papers/tu6pfp035.pdf
10. J. Wei, Y. J. Bai, J. C. Cai, et al., Proc. IPAC2010 **10**, 633 (2010).
11. T. Kubo, M. Ishihara, N. Inabe, et al., Nucl. Instrum. Methods Phys. Res. B **70** (1–4), 309 (1992). https://doi.org/10.1016/0168-583x(92)95947-p
12. U. Rucker, T. Cronert, J. Voigt, et al., Eur. Phys. J. Plus. **131** (1), 19 (2016). https://doi.org/10.1140/epjp/i2016-16019-5
13. Rutherford Appleton Laboratory Website. http://www.isis.stfc.ac.uk/.
14. P. A. Seeger, L. L. Daemen, and J. Z. Larese, Nucl. Instrum. Methods Phys. Res. A **604** (3), 719 (2009). https://doi.org/10.1016/j.nima.2009.03.204
15. R. S. Pinna, S. Rudić, S. F. Parker, et al., Nucl. Instrum. Methods Phys. Res. A **896**, 68 (2018). https://doi.org/10.1016/j.nima.2018.04.009
16. NIST Neutron News Cross Section Table **3** (3), 29 (1992); Brookhaven Database NNDC. https://www.bnl.gov/NST/NNDC.php
17. K. Kuwahara, S. Sugiyama, K. Iwasa, et al., Appl. Phys. A **74**, 302 (2002). https://doi.org/10.1007/s003390201399
18. T. Yokoo, M. Arai, K. Kuwahara, et al., Neutron News **14** (4), 18 (2010). https://doi.org/10.1080/00323910490970780
19. R. Pynn, *LANSCE (Los Alamos Neutron Science Center) Neutron Scattering a PRIMER* (Los Alamos, 1990), p. 33.
20. G. Zaccai and B. Jacrot, Annu. Rev. Biophys. Bioeng. **12** (1), 139 (1983). https://doi.org/10.1146/annurev.bb.12.060183.001035
21. D. F. R. Mildner and J. M. Carpenter, J. Appl. Crystallogr. **17** (4), 249 (1984). https://doi.org/10.1107/S0021889884011468
22. S. V. Grigor'ev, K. A. Pshenichnyi, I. A. Baraban, et al., JETP Lett. **110** 793 (12), (2019). https://doi.org/10.1134/S0370274X19240068
23. B. Jeon, J. Kim, E. Lee, et al., Nucl. Eng. Technol. **52** (3), 633 (2019). https://doi.org/10.1016/j.net.2019.08.019
24. C. M. Lavelle, *The Neutronic Design and Performance of the Indiana University Cyclotron Facility (IUCF) Low Energy Neutron Source (LENS)* (2007).
25. X. Wang, C. K. Loong, X. Guan, and T. Du, Phys. Proc. **60**, 97 (2014). https://doi.org/10.1016/j.phpro.2014.11.015
26. IPSN Website. www.aai.anl.gov/history/project_pages/ipns.html.
27. LANSCE Website. http://lansce.lanl.gov/.
28. ISIS Website. http://www.isis.stfc.ac.uk/.
29. SNS Website. http://neutrons.ornl.gov/sns.
30. JPARC Website. http://j-parc.jp/index-e.html.
31. V. L. Aksenov, V. D. Ananiev, G. G. Komyshev, et al., Phys. Part. Nucl. Lett. **14** (5), 788 (2017). https://doi.org/10.1134/S1547477117050028
32. E. Fagotti, L. Antoniazzi, D. Bortolato, et al., *Proc. IPAC2018, 2018,* p. 29. https://doi.org/10.18429/JACoW-IPAC2018-THXGBF2
33. N. Pichoff, D. Chirpaz-Cerbat, R. Cubizolles, et al., *Proc. IPAC2018, 2018,* p. 994. https://doi.org/10.18429/JACoW-IPAC2018-TUPAK015
34. C. Wiesner, S. Alzubaidi, M. Droba, et al., *Proc. IPAC2015, 2015,* p. 1276. https://doi.org/10.18429/JACoW-IPAC2015-TUXB1
35. A. Pisent, E. Fagotti, and P. Colautti, *Proc. LINAC2014, 2014,* p. 261. https://doi.org/10.18429/JACoW-LINAC2014-MOPP088
36. T. Kulevoy, R. Fatkullin, A. Kozlov, et al., *Proc. LINAC2018, 2018,* p. 349. https://doi.org/10.18429/JACoW-LINAC2018-TUPO012
37. IFMIF/EVEDA, Injector+LEBT Website. https://www.ifmif.org/?page_id155.

38. R. Hollinger, W. Barth, L. Dahl, et al., *Proc. LINAC2006, 2006,* p. 232.
39. W. D. Kilpatrick, Rev. Sci. Instrum. **28** (10), 824 (1957). https://doi.org/10.1063/1.1715731
40. A. I. Balabin and G. N. Kropachev, *Proc. EPAC1994, 1994,* p. 1180.
41. G. Kropachev, T. Kulevoy, and A. Sitnikov, J. Surf. Invest.: X-ray, Synchrotron Neutron Tech. **13** (6), 1126 (2019). https://doi.org/10.1134/S1027451019060399
42. A. Andreev and G. Parisi, *Proc. PAC1993, 1993,* p. 3124.
43. P. N. Ostroumov, N. Bultman, M. Ikegami, et al., *Proc. IPAC2018, 2018,* p. 29. https://doi.org/10.18429/JACoW-IPAC2018-THYGBF4
44. P. N. Ostroumov, *Proc. LINAC2018, 2018.* http://accelconf.web.cern.ch/AccelConf/linac2018/talks/tu2a02_talk.pdf.
45. A. Pisent, M. Cavenago, P. Bezzon, et al., *Proc. EPAC2000, 2000,* p. 1702.
46. V. Andreev, N. N. Alexeev, A. Kolomiets, et al., *Proc. EPAC2010, 2010,* p. 801. https://accelconf.web.cern.ch/IPAC10/papers/mopd052.pdf
47. V. Koshelev, G. Kropachev, T. Kulevoy, et al., *Proc. LINAC2016, 2016,* p. 575. https://accelconf.web.cern.ch/linac2016/papers/tuplr050.pdf.
48. ICIS2019 Website. https://icis2019.impcas.ac.cn/event/1/overview.

Translated by Yu. Sin'kov